




Thermal transpiration in molecular gas

Cite as: Phys. Fluids **32**, 082005 (2020); <https://doi.org/10.1063/5.0018505>

Submitted: 16 June 2020 . Accepted: 03 August 2020 . Published Online: 20 August 2020

Peng Wang (王朋) , Wei Su (苏微) , and Lei Wu (吴雷) 



View Online



Export Citation




CrossMark



NEW!

Sign up for topic alerts
New articles delivered to your inbox






Thermal transpiration in molecular gas

Cite as: Phys. Fluids 32, 082005 (2020); doi: 10.1063/5.0018505

Submitted: 16 June 2020 • Accepted: 3 August 2020 •

Published Online: 20 August 2020



Peng Wang (王朋),¹  Wei Su (苏微),²  and Lei Wu (吴雷)^{3,a)} 

AFFILIATIONS

¹State Key Laboratory of Coal Combustion, Huazhong University of Science and Technology, Wuhan 430074, China

²James Weir Fluids Laboratory, Department of Mechanical and Aerospace Engineering, University of Strathclyde, Glasgow G1 1XJ, United Kingdom

³Department of Mechanics and Aerospace Engineering, Southern University of Science and Technology, Shenzhen 518055, China

Note: This paper is part of the Special Topic, Advances in Micro/Nano Fluid Flows: In Memory of Professor Jason Reese.

^{a)}Author to whom correspondence should be addressed: wul@sustech.edu.cn

ABSTRACT

The thermal transpiration of molecular gas is investigated based on the model of Wu *et al.* [“A kinetic model of the Boltzmann equation for non-vibrating polyatomic gases,” *J. Fluid Mech.* **763**, 24–50 (2015)], which is solved by a synthetic iterative scheme efficiently and accurately. A detailed investigation of the thermal slip coefficient, Knudsen layer function, and mass flow rate for molecular gas interacting with the inverse power-law potential is performed. It is found that (i) the thermal slip coefficient and Knudsen layer function increase with the viscosity index determined by the intermolecular potential. Therefore, at small Knudsen number, gas with a larger viscosity index has a larger mass flow rate; however, at late transition and free molecular flow regimes, this is reversed. (ii) The thermal slip coefficient is a linear function of the accommodation coefficient in Maxwell’s diffuse–specular boundary condition, while its variation with the tangential momentum accommodation coefficient is complicated in Cercignani–Lampis’s boundary condition. (iii) The ratio of the thermal slip coefficients between monatomic and molecular gases is roughly the ratio of their translational Eucken factors, and thus, molecular gas always has a lower normalized mass flow rate than monatomic gas. (iv) In the transition flow regime, the translational Eucken factor continues to affect the mass flow rate of thermal transpiration, but in the free molecular flow regime, the mass flow rate converges to that of monatomic gas. Based on these results, accommodation coefficients were extracted from thermal transpiration experiments of air and carbon dioxide, which are found to be 0.9 and 0.85, respectively, rather than unity used in the literature. The methodology and data presented in this paper are useful, e.g., in the pressure correction of capacitance diaphragm gauge when measuring low gas pressures.

Published under license by AIP Publishing. <https://doi.org/10.1063/5.0018505>

I. INTRODUCTION

Thermal transpiration, where the gas moves toward a hotter region even in the absence of a pressure gradient,^{1,2} is one of the fundamental problems in rarefied gas dynamics. It has found applications in many engineering problems, including the Crookes radiometer³ that can be used in energy harvesting,^{4–6} the Knudsen compressor that pumps gas without any moving mechanical part,^{7,8} the capacitance diaphragm gauge where the effects of thermal transpiration should be subtracted for accurate measurement of low gas pressures,^{9,10} gas mixture separation,¹¹ and the Leidenfrost ratchet that rectifies the vapor flow in the boundary layer.¹²

Thermal transpiration arises when the Knudsen number Kn , defined as the ratio of mean free path λ of molecular gas to characteristic system length H , becomes appreciable in micro-/nano-devices and/or low-pressure environments.

The Boltzmann equation is adopted to study the rarefied gas dynamics. However, in engineering applications, huge computational efforts are required to obtain its numerical solutions, either deterministically^{13–15} or stochastically.^{16,17} Fortunately, when Kn is small, rarefaction effects only dominate in the Knudsen layer,¹⁸ which are reflected in terms of the velocity-slip and temperature-jump boundary conditions; hence, techniques in the computational fluid dynamics can be used to describe the rarefied gas

dynamics.^{19–21} Based on the kinetic theory, Maxwell proposed an expression for the slip velocity U at the solid surface,²

$$U \Big|_{x_2=0} = \sigma_P \frac{v_m \mu}{p} \frac{\partial U}{\partial x_2} \Big|_{x_2=0} + \sigma_T \frac{\mu}{\rho T} \frac{\partial T}{\partial x_3} \Big|_{x_2=0}, \quad (1)$$

where x_3 and x_2 are the Cartesian coordinates in the parallel and normal directions to the solid surface (see Fig. 1), respectively, while μ , ρ , T , p , and v_m are the shear viscosity, density, temperature, pressure, and most probable speed of the gas, respectively. In Eq. (1), σ_P and σ_T are the viscous slip coefficient (VSC) and thermal slip coefficient (TSC), respectively, which can be determined from the linearized Boltzmann equation (LBE)^{22–24} or from experiments.^{25–28} With the diffuse-specular boundary condition, Maxwell derived

$$\begin{aligned} \sigma_P &= \frac{2 - \alpha_M}{\alpha_M}, \\ \sigma_T &= \frac{3}{4}, \end{aligned} \quad (2)$$

where $0 \leq \alpha_M \leq 1$ is the probability of the diffuse scattering; for convenience, it will be called the tangential momentum accommodation coefficient (TMAC) in the following paper, although in addition to TMAC, the energy accommodation coefficient is also α_M . It is noted that Eq. (2) is only a rough approximation, as one would immediately ask (i) why is the TSC not a function of TMAC, (ii) how does the intermolecular potential affect the two slip coefficients in monatomic gas, and (iii) how does the internal structure of molecular (i.e., diatomic and nonlinear polyatomic) gases affect the two slip coefficients?

Extensive studies on the VSC have been carried out based on the exact or variational solutions of the LBE.^{22–24,29} It is found that the VSC is insensitive to the intermolecular potential and internal structure of molecular gases;³⁰ the latter is understandable because the internal structure of molecular gas rarely affects the shear viscosity, but the thermal conductivity.³¹ For the TSC, variational results of the LBE with Lennard-Jones and $n(r)$ -6 potentials for monatomic gases showed that the TSC depends on intermolecular potential.²⁹ Later, the same conclusion is obtained by solving the LBE with Lennard-Jones potentials accurately,^{32,33} although the TSC is indirectly fitted by expanding the mass flow rate into power series of the Knudsen number,³⁰ because the steady-state solution of LBE is

hard to find in flows with small Knudsen numbers. For this reason, the thermal transpiration is mostly studied based on simplified kinetic models.^{34–36} Since it is recognized that thermal transpiration is related to the translational thermal conductivity κ_t rather than the total thermal conductivity,^{37,38} Porodnov solved the Bhatnagar-Gross-Krook (BGK) equation³⁹ and found that the TSC can be expressed as²⁶

$$\sigma_T = \frac{3}{10} f_{tr} (1 + 0.5\alpha_M), \quad (3)$$

where

$$f_{tr} = \frac{2m\kappa_t}{3k_B\mu} \quad (4)$$

is the translational Eucken factor, with m being the molecular mass and k_B being the Boltzmann constant. For monatomic gas, we have $f_{tr} = 2.5$, and Eq. (3) is different to the original one proposed by Maxwell. For molecular gas especially some polar gases, f_{tr} can be much smaller than that of monatomic gas;³¹ therefore, it affects the thermal transpiration significantly.

It should also be noted that, based on the Hanson and Morse kinetic model⁴⁰ that is derived from the Wang-Chang and Uhlenbeck equation⁴¹ for molecular gases, the mass flow rate of thermal transpiration through channels and tubes was obtained.^{35,42,43} However, as summarized by Sharipov,³⁰ no expression other than Eq. (3) is extracted. That is to say, the role of intermolecular potential is still not known in molecular gas. Although many other kinetic models have been proposed for molecular gas,^{44–49} most of them do not take into account the velocity-dependent collision frequencies, so they can be hardly used to study the influence of intermolecular potentials.⁵⁰ On the other hand, some models do not allow a free variation of the translational Eucken factor;^{44,45} this will affect the accuracy in the extraction of gas–surface interaction parameter from thermal experiments.²⁷

Therefore, in this paper, we aim to answer how the intermolecular potential, internal structure of gas molecules, and the boundary condition affect the TSC. We will investigate the thermal transpiration of molecular gas based on the model of Wu *et al.*,⁵⁰ with the advantages that (i) the LBE for monatomic gases is recovered in the limit of no energy exchange between the translational and internal modes, and hence, the role of intermolecular potential is properly modeled; (ii) like the Rykov model,⁴⁶ the specific properties of molecular gas (e.g., bulk viscosity, translational Eucken factor, and internal thermal conductivity) can be freely adjusted, and thus, the influence of these parameter, if any, can be studied; and (iii) for low-speed flow, the efficient and accurate numerical scheme can be used to solve the Wu *et al.* model,^{14,15} while the direct simulation Monte Carlo method cannot always recover the thermal conductivity of molecular gas^{51,52} and is time-consuming when the flow velocity is far below the speed of sound.^{16,53} We will also investigate the thermal transpiration of monatomic gas, since unlike VSC, very limited data of the TSC have been reported particularly for different intermolecular potentials.

The remainder of this paper is organized as follows: In Sec. II, a synthetic iterative scheme (SIS) is developed to find the steady-state solution of the model of Wu *et al.* efficiently and accurately. In Sec. III, the SIS is used to investigate the roles of intermolecular potential and gas-surface boundary condition on the TSC, Knudsen layer function (KLF), and mass flow rate of monatomic gas. In

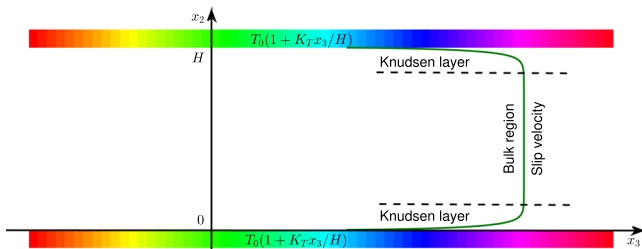


FIG. 1. Schematic of the thermal transpiration between two parallel plates, where the gas moves from the cold region to the hot region, despite the uniform gas pressure. Inside the Knudsen layer, a considerable deviation of the true velocity from the slip velocity in the bulk region is noticed; this deviation can be described by the Knudsen layer function.

Sec. IV, the SIS is applied to molecular gas, focusing on the role of translational Eucken factor. In Sec. V, reasonable accommodation coefficients were extracted by comparing numerical solutions of the model of Wu *et al.* with available experimental data on the thermal pressure difference (TPD) exponent of air and carbon dioxide. The conclusions are given in Sec. VI.

II. FORMULATION OF THE PROBLEM

Consider the steady flow of a single-species gas driven by a linear temperature gradient $K_T = Hd \ln T / dx_3$ along the x_3 direction (see Fig. 1). The gas is maintained at the same pressure along the channel, and the solid wall is stationary. The TSC and KLF will be investigated in the thermal transpiration between two infinite parallel plates located at $x_2 = 0$ and $x_2 = H$, provided that H is much larger than the mean free path of gas molecules. We will also consider the gas flow through a circular tube with a radius of H and compare our numerical results with the experimental data on the TPD exponent.

A. The kinetic model for molecular gases

The dynamics of molecular gas is described by the Wang-Chang and Uhlenbeck equation,⁴¹ where the internal structure of molecular gases makes the collision operator much more complicated than that of the Boltzmann equation for monatomic gas. Built upon the Rykov model⁴⁶ for diatomic gases, Wu *et al.* developed a kinetic model to simplify the complicated collision operator for non-vibrational molecular gases, where the numerical results showed that the influence of intermolecular potentials can be captured. For molecular gas where the vibrational modes are excited, the vibrational modes have negligible effects on the translational thermal conductivity.³¹ As the thermal transpiration is related to the translational Eucken factor only,^{37,38} which we will show in Fig. 8 below, the use of the model of Wu *et al.* is justified.

For a molecular gas with three translational and d rotational degrees of freedom, the dilute gas system is described by the one-particle velocity distribution function $f(t, \mathbf{x}, \mathbf{v}, I)$, where t is the time, $\mathbf{x} = (x_1, x_2, x_3)$ is the spatial coordinate, $\mathbf{v} = (v_1, v_2, v_3)$ is the translational velocity of gas molecules, and I is the rotational energy. It is obvious that the dependence of f on I significantly increases the computational effort; in order to improve the computational efficiency, two reduced velocity distribution functions $G(t, \mathbf{x}, \mathbf{v}) = \int_0^\infty f(t, \mathbf{x}, \mathbf{v}, I) dI$ and $R(t, \mathbf{x}, \mathbf{v}) = \int_0^\infty f(t, \mathbf{x}, \mathbf{v}, I) I^{d/2} dI$ are usually introduced to eliminate the dependence of I . For the sake of concision, we will not give the general form of the governing equations for G and R , which can be found in Ref. 50 but only present the special form for the current problem. That is, when the temperature gradient K_T is sufficiently small, we can linearize the reduced velocity distribution functions around the global equilibrium state $F_{eq}(\mathbf{v}) = \pi^{-3/2} \exp(-|\mathbf{v}|^2)$ as follows:

$$\begin{aligned} G &= F_{eq} + h_0, \\ R &= \frac{d}{2} F_{eq} + h_1. \end{aligned} \quad (5)$$

Then, introducing $h_2 = h_1 - dh_0/2$, the gas system is eventually described by the two perturbed velocity distribution functions h_0

and h_2 , whose dynamics are governed by the following equations:

$$v_1 \frac{\partial h_0}{\partial x_1} + v_2 \frac{\partial h_0}{\partial x_2} = \mathcal{L}(F_{eq}, h_0) + \delta_{rp} \Delta_G + S_0, \quad (6)$$

$$v_1 \frac{\partial h_2}{\partial x_1} + v_2 \frac{\partial h_2}{\partial x_2} = \delta_{rp} (h_2^+ - h_2) + S_2, \quad (7)$$

where h_0 and h_2 have been normalized by n_0/v_m^3 and $n_0 k_B T_0 / v_m^3$, respectively, with n_0 being the number density, T_0 being the reference temperature, and $v_m = \sqrt{2k_B T_0 / m}$ being the most probable speed. The spatial coordinates x_1 and x_2 have been normalized by H . The two source terms

$$\begin{aligned} S_0 &= -K_T v_3 \left(|\mathbf{v}|^2 - \frac{5}{2} \right) F_{eq}, \\ S_2 &= -\frac{d}{2} K_T v_3 F_{eq} \end{aligned} \quad (8)$$

are present due to the temperature gradient. Note that we have omitted the derivatives of time in Eqs. (6) and (7), since we are only interested in steady-state flow.

The two inelastic terms Δ_G and h_2^+ are supposed to describe the energy exchange between the translational and rotational motions so that the rotational temperature T_r relaxes toward the overall temperature T as $\partial T_r / \partial t = n_0 k_B T_0 (T - T_r) / Z \mu(T_0)$, where Z is the rotational collision number. However, in this specific problem, h_0 and h_2 are odd functions of v_3 , so the translational and internal temperatures are equal to the overall temperature (the wall temperature in this case). Therefore, Δ_G and h_2^+ are greatly simplified to

$$\Delta_G = \frac{4(\omega_0 - 1)}{15Z} q_{t,3} v_3 \left(|\mathbf{v}|^2 - \frac{5}{2} \right) F_{eq}, \quad (9)$$

$$h_2^+ = 2q_{r,3} v_3 F_{eq} [1 - (1 - \omega_1) / Z] (1 - \delta), \quad (10)$$

where δ is the Schmidt number of the gas. The value of Z determines the bulk viscosity of molecular gas; however, in this problem, the bulk viscosity is not important since there is no internal energy relaxation. Also note that when Z approaches infinity, Eq. (6) is reduced to the LBE for monatomic gases. The translational and rotational heat fluxes along the direction of temperature gradient, which have been normalized by $n_0 k_B T_0 v_m$, are

$$\begin{aligned} q_{t,3} &= \int h_0 \left(|\mathbf{v}|^2 - \frac{5}{2} \right) v_3 d\mathbf{v}, \\ q_{r,3} &= \int h_2 v_3 d\mathbf{v}, \end{aligned} \quad (11)$$

respectively. According to the Chapman and Cowling expansion,⁵⁴ the two constants ω_0 and ω_1 are related to the translational (κ_t) and rotational (κ_r) heat conductivities, respectively, which are given as⁵⁰

$$\kappa_t = \frac{15k_B \mu}{4m} \left(1 + \frac{1 - \omega_0}{2Z} \right)^{-1}, \quad (12)$$

$$\kappa_r = \frac{dk_B \mu}{2\delta m} \left[1 + \frac{(1 - \delta)(1 - \omega_1)}{Z\delta} \right]^{-1}. \quad (13)$$

Finally, the rarefaction parameter in Eqs. (6) and (7) is defined as

$$\delta_{rp} = \frac{n_0 k_B T_0 H}{\mu(T_0) v_m}, \quad (14)$$

and the linearized Boltzmann collision operator in Eq. (6) takes the following form:^{14,55}

$$\begin{aligned} \mathcal{L}(F_{eq}, h_0) = & \iint B [F_{eq}(\mathbf{v}') h_0(\mathbf{v}_*) + F_{eq}(\mathbf{v}_*) h_0(\mathbf{v}') \\ & - F_{eq}(\mathbf{v}) h_0(\mathbf{v}_*) - F_{eq}(\mathbf{v}_*) h_0(\mathbf{v})] d\Omega d\mathbf{v}_*. \end{aligned} \quad (15)$$

More information about the deflection angle θ , collision kernel B , and post-collision velocity \mathbf{v}' are presented in Refs. 33 and 56. In this paper, the inverse power-law potentials with the following modeled collision kernels are considered:

$$B = \frac{|\mathbf{v} - \mathbf{v}_*|^{2(1-\omega)}}{K} \sin^{\frac{1}{2}-\omega} \theta, \quad (16)$$

where ω is the viscosity index⁵⁷ and K is the normalization constant.^{14,33} The slower the inverse power-law potential decays with respect to the intermolecular distance, the larger the value of ω . For instances, hard-sphere (HS) and Maxwellian molecules have $\omega = 0.5$ and 1, respectively. For polar gases dominated by dipole interactions, we have $\omega = 1.5$. Note that although realistic potential can be used, the TSC and KLF are determined by the effective viscosity index ω .²⁴

In the following calculations, we set $K_T = 1$ in Eq. (8). The macroscopic flow velocity that is normalized by the most probable speed is calculated as $U_3(x_1, x_2) = \int h_0 v_3 d\mathbf{v}$. The KLF, which is the defect velocity U_d inside the Knudsen layer, is retrieved through the thermal transpiration along straight planar channel according to the following equation (see Fig. 1):

$$U_d \left(\frac{x_2}{Kn} \right) = \frac{1}{Kn} \left[U_3 \left(x_2 = \frac{1}{2} \right) - U_3(x_2) \right], \quad (17)$$

where the Knudsen number is formally defined as $Kn = \lambda/H = \sqrt{\pi}/2\delta_{rp}$. Meanwhile, the TSC is calculated as

$$\sigma_T = 2\delta_{rp} U_3 \left(x_2 = \frac{1}{2} \right). \quad (18)$$

Note that δ_{rp} should be set large enough to avoid the overlap of the two Knudsen layers in the vicinity of the plates.

B. Gas kinetic boundary conditions

The gas–surface boundary condition is needed in spatially inhomogeneous problems. The general form of the boundary condition, which specifies the relation between the velocity distribution function f of the reflected and incident gas molecules at the boundary via a non-negative scattering kernel $R(\mathbf{v}' \rightarrow \mathbf{v})$, is given as follows:

$$v_n f(\mathbf{v}) = \int_{v'_n < 0} |v'_n| R(\mathbf{v}' \rightarrow \mathbf{v}) f(\mathbf{v}') d\mathbf{v}', \quad v_n > 0, \quad (19)$$

where \mathbf{v}' and \mathbf{v} are the velocities of the incident and reflected molecules, respectively, and v_n is the normal component of the molecular velocity \mathbf{v} directed into the gas.

The most popular gas–surface boundary condition is the Maxwell or diffuse-specular one, with the scattering kernel reading as

$$\begin{aligned} R_M(\mathbf{v}' \rightarrow \mathbf{v}) = & \alpha_M \frac{m^2 v_n}{2\pi(kT_w)^2} \exp\left(-\frac{m|\mathbf{v}'|^2}{2kT_w}\right) \\ & + (1 - \alpha_M) \delta_d(\mathbf{v}' - \mathbf{v} + 2\mathbf{n}v_n), \end{aligned} \quad (20)$$

where δ_d is the Dirac delta function. The boundary condition assumes that, after collision with the surface, a molecule is specularly reflected with the probability $1 - \alpha_M$; otherwise, it is scattered diffusely (i.e., reflected toward every direction with equal probability in a Maxwellian velocity distribution). Purely diffuse reflection takes place when $\alpha_M = 1$.

In addition to the Maxwell model, the Cercignani–Lampis (CL) boundary condition has also been widely used.^{58,59} For simplicity in this paper, we consider the case where the energy accommodation coefficient associated with the rotational modes is one so that the scattering kernel reads

$$\begin{aligned} R_{CL}(\mathbf{v}' \rightarrow \mathbf{v}) = & \frac{m^2 v_n}{2\pi\alpha_n\alpha_t(2 - \alpha_t)(kT_w)^2} I_0 \left(\frac{\sqrt{1 - \alpha_n} m v_n v'_n}{\alpha_n k T_w} \right) \\ & \times \exp \left\{ -\frac{m[v_n^2 + (1 - \alpha_n)v'_n]^2}{2kT_w\alpha_n} \right. \\ & \left. - \frac{m[\mathbf{v}_t - (1 - \alpha_t)\mathbf{v}'_t]^2}{2kT_w\alpha_t(2 - \alpha_t)} \right\}, \end{aligned} \quad (21)$$

where \mathbf{v}_t is the tangential component of the molecular velocity, $I_0(x) = \frac{1}{2\pi} \int_0^{2\pi} \exp(x \cos \phi) d\phi$, $0 \leq \alpha_n \leq 1$ is the energy accommodation coefficient, and $0 \leq \alpha_t \leq 2$ is the effective TMAC. When $\alpha_n = \alpha_t = 1$ or $\alpha_n = \alpha_t = 0$, the fully diffuse or specular boundary conditions are recovered, respectively.

With these boundary conditions, it can be found that for the thermal transpirations between two parallel plates and along the straight long tube, the mass flow rate or the flow velocity U_3 that is mainly concerned to recover the KLF and TSC is only determined by Eq. (6). In other words, the mass flow rate is determined by the rarefaction parameter δ_{rp} , the intermolecular potential that is reflected by the viscosity index ω in Eq. (16), and $(\omega_0 - 1)/Z$; the last parameter is related to the translational Eucken factor in the following manner:

$$f_{tr} = \frac{2 m \kappa_t}{3 k_B \mu} = \frac{5}{2} \left(1 + \frac{1 - \omega_0}{2Z} \right)^{-1}. \quad (22)$$

C. The synthetic iteration scheme

The steady-state solution of Eq. (6) is normally found by the conventional iteration scheme. Given $h_0^{(k)}(x_1, x_2, \mathbf{v})$ at the k th iteration step, its value at the next iteration step is calculated by solving the following equation:⁵⁰

$$\begin{aligned} v h_0^{(k+1)} + v_1 \frac{\partial h_0^{(k+1)}}{\partial x_1} + v_2 \frac{\partial h_0^{(k+1)}}{\partial x_2} \\ = \mathcal{L}(F_{eq}, h_0^{(k)}) + \delta_{rp} \Delta_G^{(k)} + v h_0^{(k)} + S_0, \end{aligned} \quad (23)$$

where the constant ν is roughly equal to $\delta_{rp}(Z+1)/Z$ to make the iteration stable, the spatial derivative is approximated by a second-order upwind finite difference, and the linearized Boltzmann collision operator in Eq. (15) is calculated by the fast spectral method.³³ The process is repeated until relative differences between successive estimates of macroscopic quantities are less than a convergence criterion.

The conventional iteration scheme is efficient for highly rarefied gas flows, where converged solutions can be found after several iterations. However, the number of iterations increases significantly with δ_{rp} , especially when the gas flow is in the near-continuum regime. To expedite the convergence, synthetic equations for macroscopic quantities should be developed and solved together with the kinetic equation.⁶⁰ Since the flow velocity U_3 is the primary concern here, we consider the following synthetic equation to boost the convergence significantly:⁶¹

$$\frac{\partial^2 U_3}{\partial x_1^2} + \frac{\partial^2 U_3}{\partial x_2^2} = -\frac{1}{4} \left(\frac{\partial^2 F_{2,0,1}}{\partial x_1^2} + 2 \frac{\partial^2 F_{1,1,1}}{\partial x_1 \partial x_2} + \frac{\partial^2 F_{0,2,1}}{\partial x_2^2} \right) + 2 \frac{\partial}{\partial x_1} \int v_1 v_3 \mathcal{L}' dv + 2 \frac{\partial}{\partial x_2} \int v_2 v_3 \mathcal{L}' dv, \quad (24)$$

where $\mathcal{L}' = \mathcal{L} + \delta_{rp} \Delta_G + \delta_{rp} h_0$ and $F_{l_1, l_2, l_3}(x_1, x_2) = \int h_0 H_{l_1}(v_1) H_{l_2}(v_2) H_{l_3}(v_3) dv$, with $H_n(v)$ being the n th order physicist's Hermite polynomial. Based on the synthetic equation (24), we propose the following synthetic iteration scheme (SIS):

- When $h_0^{(k)}$, $U_3^{(k)}$, and $q_{t,3}^{(k)}$ are known at the k th iteration step, we calculate $\int v_1 v_3 \mathcal{L}' dv$ and $\int v_2 v_3 \mathcal{L}' dv$ in Eq. (24). We also calculate the distribution function $h_0^{(k+1/2)}$ at the intermediate step by solving the following equation:

$$\nu h_0^{(k+1/2)} + v_1 \frac{\partial h_0^{(k+1/2)}}{\partial x_1} + v_2 \frac{\partial h_0^{(k+1/2)}}{\partial x_2} = \mathcal{L}(F_{eq}, h_0^{(k)}) + \delta_{rp} \Delta_G^{(k)} + \nu h_0^{(k)} + S_0. \quad (25)$$

- From $h_0^{(k+1/2)}$, we calculate the flow velocity $U_3^{(k+1/2)}$ and $F_{2,0,1}$, $F_{1,1,1}$, and $F_{0,2,1}$. Near the solid surface, we let $U_3^{(k+1)} = U_3^{(k+1/2)}$, while the flow velocity $U_3^{(k+1)}$ in the bulk region is obtained by solving the diffusion-type Eq. (24).
- A correction of the velocity distribution function is introduced in accordance with the changed flow velocity,

$$h_0^{(k+1)} = h_0^{(k+1/2)} + 2(U_3^{(k+1)} - U_3^{(k+1/2)})v_3 F_{eq}. \quad (26)$$

- The above steps are repeated until convergence.

D. Numerical efficiency

Note that when $Z \rightarrow \infty$, there is no translational–rotational energy transfer so that Eq. (6) degenerates to the LBE for monatomic gases, for which the accuracy and efficiency of SIS have been demonstrated.⁶¹ Here, we consider the performance of SIS for the thermal transpiration of a diatomic gas between two infinite parallel plates located at $x_2 = 0$ and $x_2 = 1$, respectively.

To solve Eq. (6), v_1 and v_3 are discretized by 32×32 uniform grids in the range of $[-6, 6]$, while v_2 is discretized non-uniformly by

$$v_2 = 6 \frac{(-N_\nu + 1, -N_\nu + 3, \dots, N_\nu - 1)^t}{(N_\nu - 1)^t}, \quad (27)$$

with most of the discrete velocities located near $v_2 \sim 0$ to capture the discontinuity in the velocity distribution function; we take $N_\nu = 128$ and $t = 5$. In order to capture the Knudsen layer near the solid surface, the spatial domain $0 \leq x_2 \leq 1/2$ is divided into N_s non-uniform sections, with most of the discrete points placed in the vicinity of solid surface,

$$x_2 = (10 - 15s + 6s^2)s^3, \quad s = \frac{(0, 1, \dots, N_s)}{2N_s}. \quad (28)$$

Due to symmetry $h_0(x_2, v_1, v_2, v_3) = h_0(1 - x_2, v_1, -v_2, v_3)$, the other half spatial domain is not considered. In this test, we choose $N_s = 100$. In the fast spectral approximation of the linearized Boltzmann collision operator (15), the integral with respect to the solid

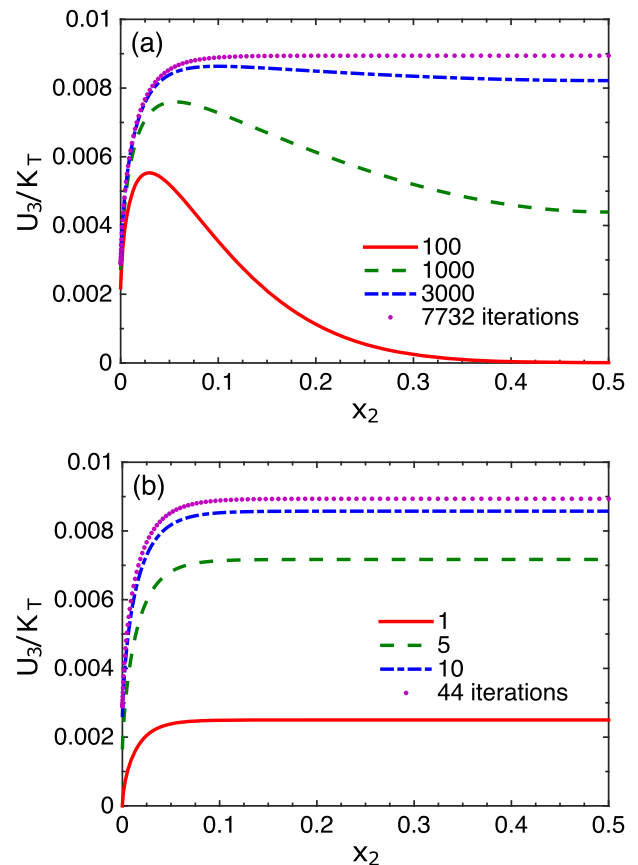


FIG. 2. Velocity profiles at different iteration steps obtained from the conventional iteration scheme (a) and SIS (b) when $\delta_{rp} = 50$. The HS diatomic molecules with $d = 2$, the Schmidt number $\delta = 1/1.33$, and the rotational collision number $Z = 2$ are considered. The initial condition is $h_0(x_2, \mathbf{v}) = 0$. The iteration is terminated when the maximum relative difference in the flow velocity between two consecutive iterations is less than 10^{-6} .

angle Ω is calculated by the Gauss–Legendre quadrature with $M = 8$ [see Eq. (39) in Ref. 56].

Figure 2 compares the convergence history of SIS to that of the conventional iteration scheme when $\delta_{rp} = 50$. Starting from the zero initial condition, the perturbation induced by the temperature gradient at the solid surface slowly penetrates the bulk regime in the conventional iteration scheme such that the converged solution is reached after 7732 iteration steps. This situation is completely changed in SIS, where the flow velocity is corrected according to the synthetic equation (24). Such a macroscopic governing equation allows the efficient exchange of information in the whole computational domain, and therefore, fast convergence is realized after only 44 iteration steps. The gain of using SIS becomes larger as δ_{rp} further increases. Since the computational effort to solve the synthetic equation is negligible compared to that of the kinetic equation [i.e., for the LBE, the computational cost is proportional to $N_s N_v^3 \log(N_v)$, while for the synthetic equation, it is proportional to N_s^2], the computational time saving in the SIS is proportional to the number of iterations it saves. At $\delta_{rp} = 200$, the SIS is about 500 times more efficient than the conventional iteration scheme. Such an efficient scheme facilitates the calculation of TSC and KLF over a wide range of parameters.

Note that the SIS is particularly devised for the linearized thermal transpiration to achieve fast convergence to the steady-state solution in the near-continuum regime, where the direction of the flow velocity U_3 is perpendicular to the computational domain $x_1 - x_2$ and only one synthetic diffusion-type equation for U_3 is needed. We have also developed the general synthetic iterative scheme that can boost the convergence of general rarefied gas flow in all the flow regimes,^{15,62} and the method is ready to be extended to general molecular gas flows.

III. NUMERICAL RESULTS OF MONATOMIC GASES

We first consider the thermal transpiration of monatomic gas between two parallel plates. Since some LBE solutions are available in the literature for HS molecules,^{23,30} the accuracy of SIS and the fast spectral method for the Boltzmann collision operator (15) can be further validated.

In our simulations, the rarefaction parameter δ_{rp} is set as 100 so that the wall distance is about 100 times larger than the molecular mean free path. Thus, the interference between two Knudsen layers near the plates is avoided. To solve Eq. (6), the discretization of molecular velocity space is the same as that used in Sec. II D. In order to capture the sharp variation of the velocity profile inside the Knudsen layer, we choose $N_s = 500$ for the spatial discretization in Eq. (28). All these measures enable our results to hold an accuracy to the sixth decimals.²⁴

A. The thermal slip coefficient

Unlike the VSC, very little data of the TSC have been obtained from the LBE, particularly the TSCs for different intermolecular potentials. Here, we close this gap by solving the LBE via the SIS for different intermolecular potentials and gas–surface interactions.

We first solve the LBE for HS molecules with the diffuse–specular boundary condition and compare the TSC with those

obtained by Wakabayashi *et al.*⁶³ and Siewert.⁶⁴ We find that the three groups of data agree well with each other, and especially, the relative difference between our results and those of Siewert⁶⁴ is less than 10^{-3} ; this confirms the accuracy of our method.

Figure 3 shows the variation of TSC with respect to the TMAC α_M for different types of intermolecular potential. When α_M is fixed, it is seen in most cases that the TSC increases with the viscosity index, except that this trend is reversed when α_M approaches zero. When the intermolecular potential is fixed, we find that the data obtained from the LBE can be approximately fitted by linear functions of α_M , with the relative discrepancy between fitting results and numerical data being less than 1.5%, and the slope of fitting increases with the viscosity index.

Table I and Fig. 4 summarize the TSC computed from the LBE for HS, Maxwellian, and variable hard sphere (VHS) ($\omega = 1.5$) molecules with the CL boundary condition. When α_t and α_n are fixed, the TSC increases with the viscosity index. For example, when the HS and VHS with $\omega = 1.5$ are considered, the maximum relative difference reaches 58% when $\alpha_t = 2$ and $\alpha_n = 1$. When the viscosity index is fixed, however, the variation of TSC with respect to the effective TMAC α_t and energy accommodation coefficient α_n is complicated. We first consider the case when the values of α_t and the intermolecular potential are fixed. From Table I, we see that, when $\alpha_t < 1$, the TSC increases with α_n where the maximum increment is less than 20% when α_n varies from 0.25 to 1. Furthermore, this kind of variation reduces when α_t approaches 1; when $\alpha_t = 1$, the CL boundary condition is reduced to the fully diffuse one in this problem, and the TSC does not vary with α_n . When $\alpha_t > 1$, the variation of TSC on α_n reverses when compared to that of $\alpha_t < 1$. We then fix the value of α_n and the intermolecular potential to see how α_t affects the TSC. Unlike the diffuse–specular boundary condition where the TSC is nearly a linear function of TMAC, here, the change in the TSC with respect to α_t is nonlinear. Also, it is observed that the smaller the value of α_n , the stronger the variation in the TSC with α_t . For instance, when $\omega = 0.5$ and $\alpha_n = 0.75$, the TSC first decreases to a minimum value at $\alpha_t \approx 0.5$ and then increases to a maximum value

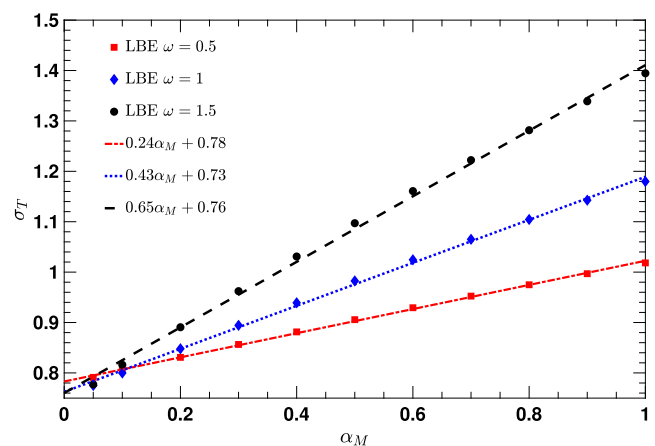


FIG. 3. Symbols: TSCs obtained from the LBE for HS, Maxwellian, and variable hard sphere (VHS, $\omega = 1.5$) molecules when the diffuse–specular boundary condition is used. Lines: linear fittings of TSCs with respect to the TMAC.

TABLE I. TSCs obtained from the LBE for HS, Maxwellian, and VHS ($\omega = 1.5$) molecules under the CL boundary condition with different values of the effective TMAC α_t and energy accommodation coefficient α_n .

α_t	ω	$\alpha_n = 0.25$	$\alpha_n = 0.5$	$\alpha_n = 0.75$	$\alpha_n = 1$
0.25	0.5	0.878 961	0.939 289	0.997 097	1.052 749
	1.0	0.957 507	1.031 589	1.103 622	1.173 821
	1.5	1.073 727	1.166 016	1.256 071	1.343 934
0.5	0.5	0.915 032	0.953 837	0.991 52	1.028 174
	1.0	1.038 391	1.085 497	1.132 079	1.178 087
	1.5	1.207 714	1.265 554	1.323 069	1.380 077
0.75	0.5	0.963 946	0.982 787	1.001 310	1.019 504
	1.0	1.111 326	1.134 018	1.156 801	1.179 587
	1.5	1.309 165	1.336 765	1.364 675	1.392 753
1.0	0.5	1.018 280	1.018 280	1.018 280	1.018 280
	1.0	1.179 794	1.179 794	1.179 794	1.179 794
	1.5	1.394 533	1.394 533	1.394 533	1.394 533
1.25	0.5	1.070 999	1.053 104	1.035 091	1.017 060
	1.0	1.245 767	1.224 484	1.202 513	1.180 003
	1.5	1.476 314	1.450 674	1.423 957	1.396 309
1.5	0.5	1.114 835	1.079 992	1.044 506	1.008 646
	1.0	1.310 156	1.269 058	1.226 052	1.181 462
	1.5	1.564 814	1.515 439	1.463 286	1.408 579
1.75	0.5	1.142 984	1.092 304	1.040 058	0.986 740
	1.0	1.372 910	1.313 785	1.251 073	1.185 256
	1.5	1.667 706	1.596 793	1.520 959	1.440 373
2	0.5	1.150 836	1.085 729	1.017 732	0.947 616
	1.0	1.433 179	1.358 215	1.277 626	1.191 998
	1.5	1.788 740	1.698 623	1.601 268	1.496 587

at $\alpha_t \approx 1.5$. This is not observed in the work⁶⁵ where the Shakhov gas kinetic model,⁶⁶ which is a simplified version of the Boltzmann equation, is employed, and the TSC always increases with α_t when α_n is fixed.

B. The Knudsen layer function

The influence of intermolecular potential on the KLF has been rarely studied, even for monatomic gases, due to the complexity of the Boltzmann collision operator and the lack of efficient numerical methods to simulate the near-continuum flow. However, as will be shown in Sec. III C, the KLF is important as it is closely related to the second-order correction (in terms of the Knudsen number) to the mass flow rate. Fortunately, these computational difficulties can be tackled by the fast spectral method³³ and the SIS in Sec. II C.

Figure 5 shows the KLF obtained from the LBE for HS, Maxwellian, and VHS ($\omega = 1.5$) molecules when the diffuse boundary condition is applied. Obviously, the KLF is strongly affected by the intermolecular potential, i.e., its value increases with the viscosity index ω . For example, the value of the KLF at the solid surface for VHS molecules with $\omega = 1.5$ is larger than that of the HS molecules by approximately 60%.

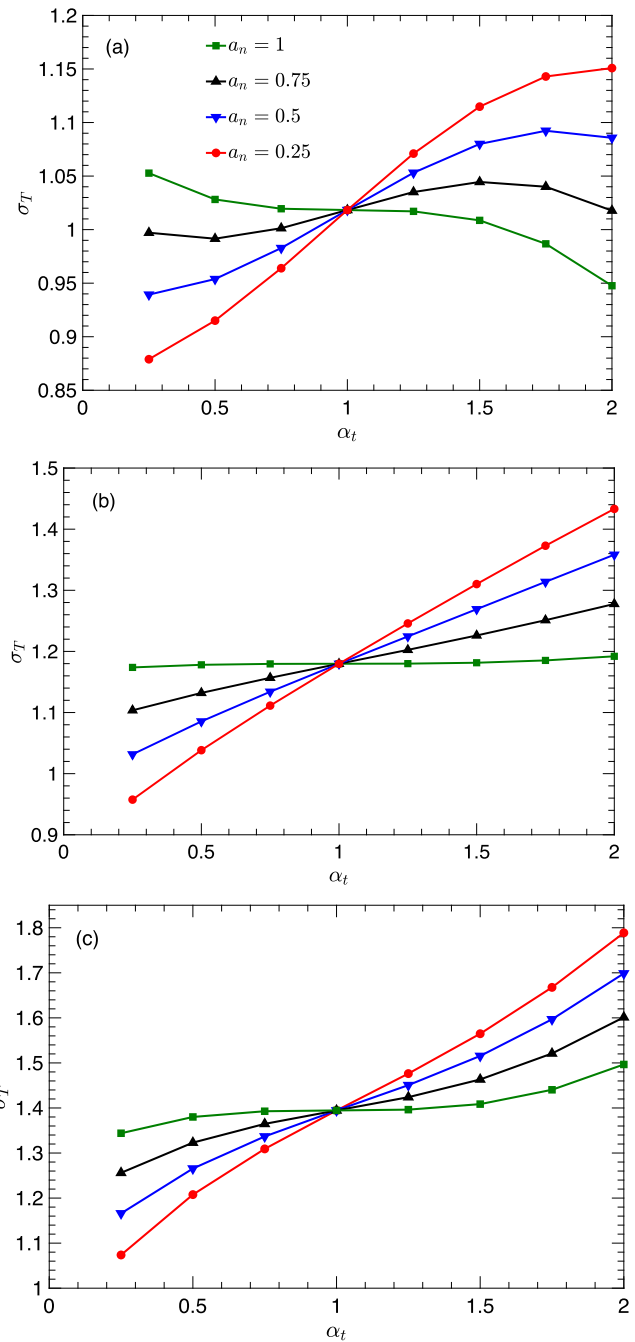


FIG. 4. TSCs obtained from LBE for (a) HS, (b) Maxwellian, and (c) VHS ($\omega = 1.5$) molecules when the CL boundary condition is used.

Figure 6(a) further depicts the KLF when the specular–diffuse boundary condition is used from the case of $\alpha_M = 0.2$ where the specular reflection is strong. It is noticed that the KLF decreases with the TMAC; this is in sharp contrast to the KLF in Kramer’s problem where its value increases when the TMAC decreases.²⁴ However,

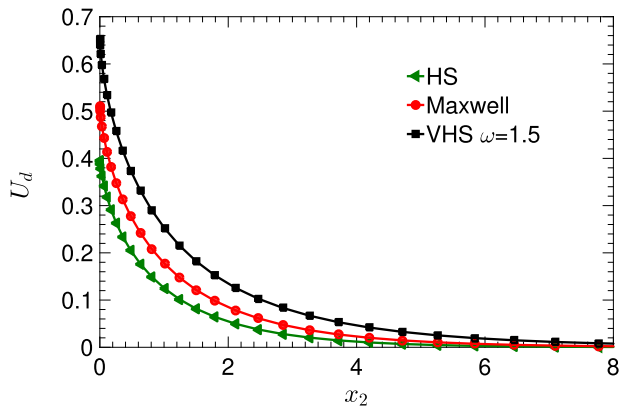


FIG. 5. KLFs obtained from the LBE for HS, Maxwellian, and VHS ($\omega = 1.5$) molecules when the diffuse boundary condition is applied.

both the thermal transpiration and Couette flow possess the singularity of the velocity gradient at the planar surface. That is, dU_d/dx_2 varies as $x_2 \ln x_2$ in the vicinity of the wall, and such a gradient divergence is general in rarefied gas dynamics.^{67,68} This conclusion holds also in the Couette flow described by the BGK kinetic model,⁶⁹ where the asymptotic analysis demonstrates that the KLF near the boundary can be described by the following power series:

$$\frac{U_d(x_2)}{U_d(0)} = \sum_{n=0}^2 \sum_{m=0}^2 c_{n,m} x_2^n (x_2 \ln x_2)^m. \quad (29)$$

Interestingly, through numerical simulation and fitting, we find that the KLF in thermal transpiration can also be perfectly fitted by the same function, where the fitting coefficients are listed in Table II.

Under the diffuse–specular boundary condition, the similarity of KLF is found in Fig. 6(b); that is, when the KLFs are rescaled by their values on the solid surface, they almost overlap with each other. As shown in the inset, the maximum relative difference among all the TMACs is less than 4%. Thus, the KLF for the diffuse–specular boundary condition holds a good similarity at different values of TMAC. This happens not only for HS molecules but also for other intermolecular potentials (not shown). Furthermore, we find that the value of KLF on the solid surface $x_2 = 0$ can be fitted by using an exponential function of α_M ,

$$U_d(0) = c_1 [1 - \exp(-c_2 \alpha_M)], \quad (30)$$

where the fitting coefficients c_1 and c_2 are shown in Table II.

The KLFs are also obtained from the LBE with the CL boundary condition. When α_t and α_n are fixed, the KLF increases with the viscosity index. However, unlike the diffuse–specular boundary condition, the KLF only exhibits weak similarities when either α_t or α_n is fixed (not shown here).

C. Mass flow rate: The second-order contribution from KLF

It is very hard to measure the TSC and KLF directly; instead, the mass flow rate and TPD exponent are measured. Since the TPD

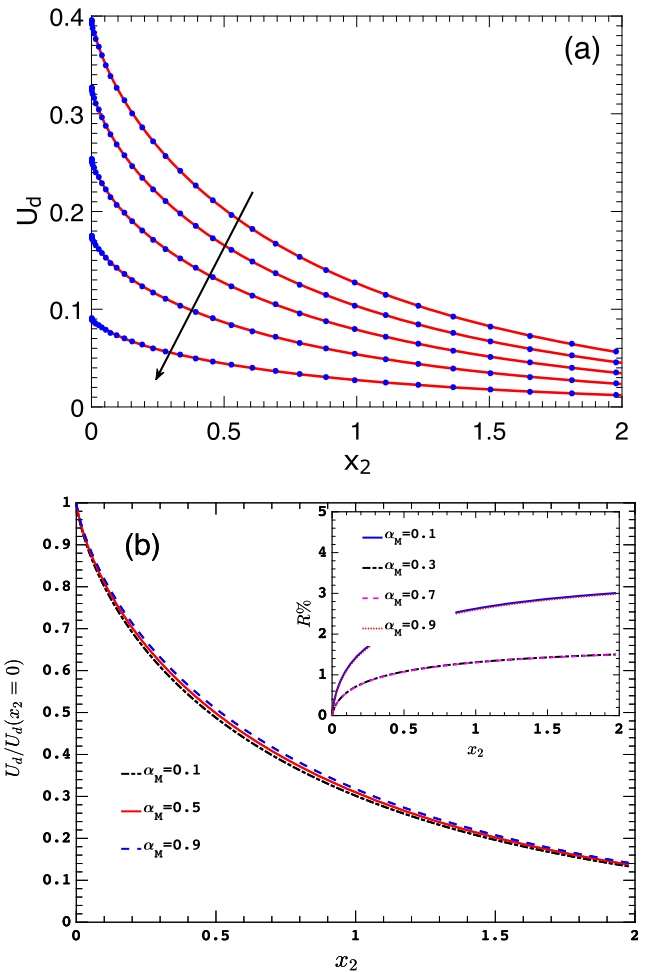


FIG. 6. (a) KLFs for HS molecules with the diffuse–specular boundary condition. Along the arrow, the TMAC is $\alpha_M = 1.0, 0.8, 0.6, 0.4,$ and $0.2,$ respectively. Solid lines—LBE results and dots—fitting results by Eq. (29). (b) The rescaled KLF $U_d(x_2)/U_d(0)$ when the HS molecules and diffuse–specular boundary condition are used. For clarity, results at other values of α_M are not shown. Inset: the relative difference of the rescaled KLF for various α_M when compared to that of $\alpha_M = 0.5$.

exponent is strongly related to the mass flow rate, here, we quantify the influence of intermolecular potential and gas–surface boundary condition on the mass flow rate in the near-continuum and early transition flow regimes.

When δ_{rp} is large such that the two Knudsen layers do not overlap, from Eqs. (17) and (18), we find that the normalized mass flow rate Q can be calculated exactly as

$$Q = \frac{\sigma_T}{2\delta_{rp}} - \frac{\pi}{4\delta_{rp}^2} Q_d, \quad (31)$$

where

$$Q_d = \int_0^\infty U_d(x_2) dx_2 \quad (32)$$

TABLE II. Fitting coefficients of the rescaled KLF (29) and $U_d(0)$ in Eq. (30) for inverse power-law potentials with different values of viscosity index ω when the diffuse boundary condition is used. Note that the coefficient $c_{0,0}$ is always 1 and the area under the KLF is $Q_d = \int_0^\infty U_d(x_2) dx_2$.

ω	$c_{0,1}$	$-c_{0,2}$	$c_{1,0}$	$c_{1,1}$	$-c_{1,2}$	$-c_{2,0}$	$c_{2,1}$	$100c_{2,2}$	c_1	c_2	$Q_d/U_d(0)$
0.5	0.7902	0.1898	0.2116	0.4360	0.0337	0.9019	0.090 16	0.1226	1.364	0.3422	1.9164
0.75	0.9344	0.3722	0.7415	0.6773	0.0864	1.4200	0.2145	0.3768	1.365	0.4004	2.0306
1.0	1.1070	0.5903	1.3790	0.9858	0.1394	2.0450	0.3499	0.5672	1.401	0.4520	2.1724
1.25	1.3910	1.0960	2.5070	1.3990	0.3177	3.1590	0.7581	1.4590	1.468	0.4964	2.3465
1.5	1.7550	1.8140	4.0150	1.9330	0.5663	4.6510	1.3420	2.5580	1.562	0.5360	2.5800

is the mass flow rate correction due to defect velocity, whose values for typical values of viscosity index are listed in Table III when the CL boundary condition is used. When the diffuse-specular boundary condition is used, Q_d can be recovered by using the data in the last three columns in Table II and Eq. (30). It is seen from Eq. (31) that the KLF provides a correction of the mass flow rate up to the second-order of the Knudsen number.

The comparison of the mass flow rate computed from the LBE and Eq. (31) for HS and Maxwellian molecules is shown in Fig. 7.

TABLE III. The area of the Knudsen layer function Q_d for various intermolecular potentials when the CL boundary condition is used. Results of $\alpha_t = 1$ are not shown as Q_d are the same as those from the diffuse boundary conditions in Table II, irrespective of the value of α_n .

α_t	ω	$\alpha_n = 0.25$	$\alpha_n = 0.5$	$\alpha_n = 0.75$	$\alpha_n = 1$
0.25	0.5	0.3730	0.4926	0.6081	0.7201
	1.0	0.5648	0.7140	0.8580	0.9973
	1.5	0.8827	1.0901	1.2869	1.4729
0.5	0.5	0.5219	0.5987	0.6738	0.7472
	1.0	0.7967	0.8922	0.9855	1.0767
	1.5	1.2432	1.3741	1.4995	1.6192
0.75	0.5	0.6462	0.6836	0.7204	0.7568
	1.0	0.9675	1.0138	1.0595	1.1047
	1.5	1.4883	1.5511	1.6119	1.6705
1.25	0.5	0.8672	0.8314	0.7955	0.7595
	1.0	1.2454	1.2014	1.1571	1.1125
	1.5	1.8609	1.8013	1.7427	1.6849
1.5	0.5	0.9813	0.9114	0.8405	0.7688
	1.0	1.4008	1.3149	1.2280	1.1396
	1.5	2.0828	1.9655	1.8497	1.7345
1.75	0.5	1.1063	1.0041	0.8997	0.7930
	1.0	1.5928	1.4678	1.3405	1.2100
	1.5	2.3807	2.2069	2.0352	1.8631
2	0.5	1.2439	1.1121	0.9762	0.8361
	1.0	1.8312	1.6699	1.5052	1.3351
	1.5	2.7784	2.5475	2.3196	2.0905

Note that the mass flow rate $Q_1 = \sigma_T/2\delta_{rp}$ obtained from the analytical solution with the first-order thermal slip boundary condition is also plotted in the figure. It is clear that the mass flow rate computed from Q_1 is only in good agreement with the LBE result at a large value of $\delta_{rp} \geq 100$, while that from Eq. (31) agrees well with the LBE results of Q in the interval of $\delta_{rp} \geq 5$. For example, in the case of $\delta_{rp} = 5$, when compared with results of LBE for HS molecules, the relative error in the mass flow rate for Eq. (31) is smaller than 5%, while it is larger than 40% for Q_1 . The reason that Eq. (31) does not work well when $\delta_{rp} < 5$ is that the KLFs at two solid surfaces start to overlap and higher-order corrections are needed.

Although the TSC increases with the viscosity index when other parameters are fixed, the KLF and hence Q_d also increase with the viscosity index. Therefore, from (31), it may be concluded that at large values of the Knudsen number, gas with a smaller value of viscosity index may have a larger mass flow rate. This is observed in Fig. 10 below when $Kn > 0.6$.

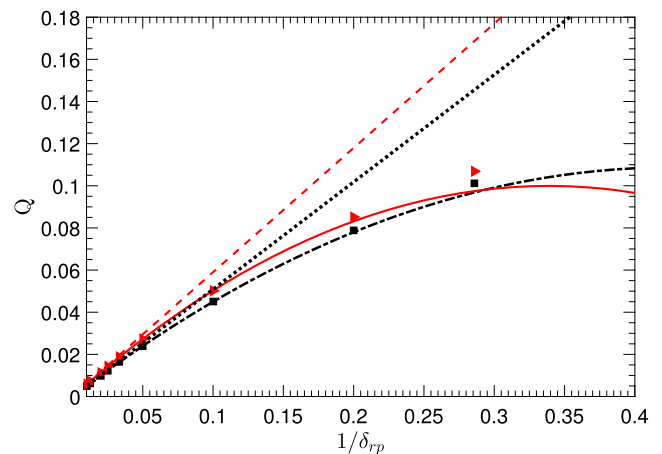


FIG. 7. The normalized mass flow rate Q vs $1/\delta_{rp}$ when the diffuse boundary condition is used. Squares, dashed-dotted line, and dot line represent the results of HS molecules calculated from the LBE [Eq. (31)] and the analytical solution with the first-order slip boundary condition (i.e., $Q_1 = \sigma_T/2\delta_{rp}$), respectively. Triangles, solid line, and dashed line are the corresponding results for Maxwellian molecules.

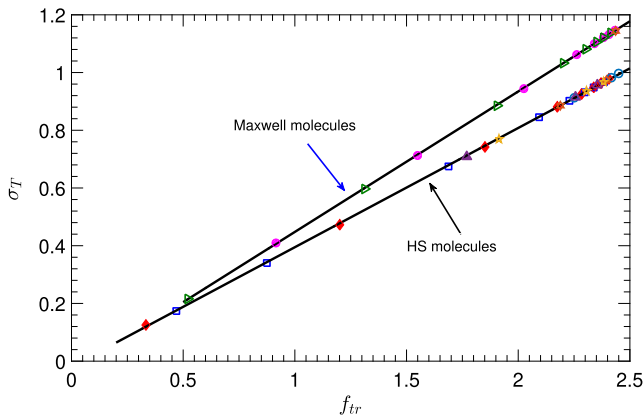


FIG. 8. TSCs vs the translational Eucken factor f_{tr} for molecular gas when the diffuse boundary condition is applied. Solid diamonds—HS molecules, $\delta^{-1} = 1.2$, $d = 2$, hollow squares—HS molecules, $\delta^{-1} = 1.2$, $d = 3$, solid circles—Maxwellian molecules, $\delta^{-1} = 1.55$, $d = 2$, hollow triangles—Maxwellian molecules, $\delta^{-1} = 1.55$, $d = 3$, hollow circles—HS molecules, $\delta^{-1} = 2$, $d = 2$, hollow hexagrams—HS molecules, $\delta^{-1} = 2$, $d = 3$, solid pentagrams—HS molecules, $\delta^{-1} = 1.33$, $d = 2$, and solid triangles— $\delta^{-1} = 1.33$, $d = 3$. Solid lines are the linear fitting solutions.

IV. NUMERICAL RESULTS OF MOLECULAR GASES

So far, no work has been devoted to finding the TSC and KLF of molecular gases based on the Boltzmann equation,³⁰ although they can be roughly extracted from the numerical data given by Loyalka *et al.*⁴² and Lo and Loyalka,⁴³ where the thermal transpiration of molecular gases along planar channels and circular tubes was calculated based on the model of Hanson and Morse kinetic.⁴⁰ However, this model is proposed only for Maxwellian molecules ($\omega = 1$), so the influence of intermolecular potential cannot be captured. In the following, we report the details on the TSC and KLF obtained from the model of Wu *et al.*⁵⁰ Discretizations of spatial space and molecular velocity space are the same as those in Sec. III.

A. The thermal slip coefficient

We first consider the diffuse boundary condition and solve the model of Wu *et al.* for diatomic ($d = 2$) and nonlinear polyatomic ($d = 3$) gases. Although in the last paragraph of Sec. II, we have stated

TABLE IV. When the diffuse-specular boundary condition is applied, the TSC of molecular gases can be fitted according to Eq. (33), where the fitting coefficients depend on the intermolecular potential.

ω	C_1	C_2
0.5	0.095	0.310
0.75	0.125	0.309
1.0	0.165	0.305
1.25	0.202	0.304

that the thermal transpiration along straight planar channel/tube is determined by the intermolecular potential (viscosity index), the rarefaction parameter (or Knudsen number), and translational Eucken factors, here, we solve the kinetic equations (6) and (7) with different combinations of the Schmidt number δ , rotational number Z , ω_0 , and ω_1 to see their influences. From Fig. 8, it is found that, for HS and Maxwell molecules with diffuse boundary condition, all the TSCs fall in a straight lines when plotted against the translational Eucken number f_{tr} , which indicates that the TSC is indeed determined by ω and f_{tr} .

We further repeat the numerical simulations using different values of TMAC α_M and continue to find that σ_T is a linear function of f_{tr} when α_M and intermolecular potential are fixed. From a practical perspective, a more accurate relationship among σ_T , α_M ,

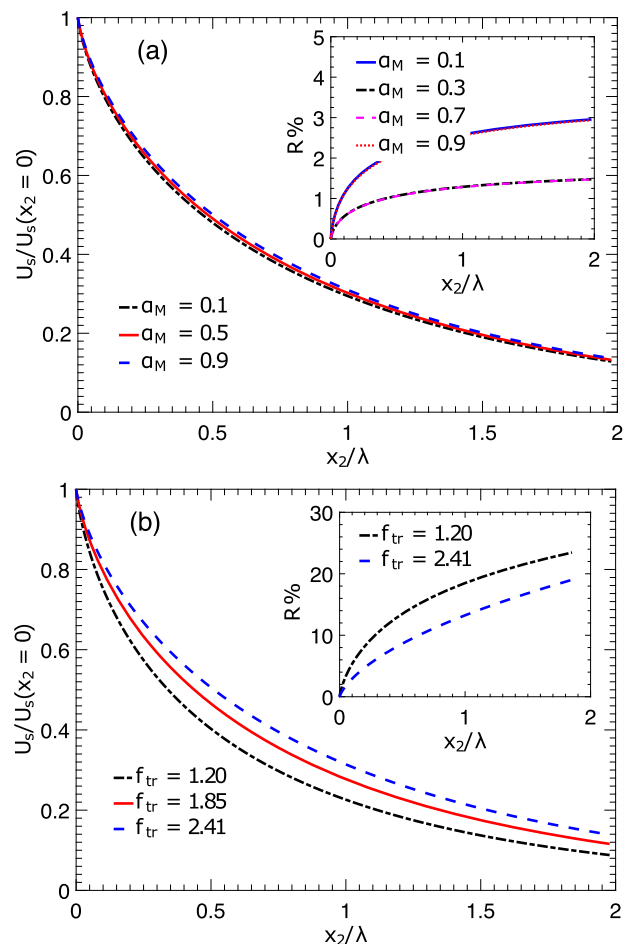


FIG. 9. The rescaled KLF $U_s(x_2)/U_s(0)$ obtained from the model of Wu *et al.*⁵⁰ for the HS molecules subject to the diffuse-specular boundary condition. (a) The diffuse-specular boundary condition at different α_M is applied with $f_{tr} = 2.37$. Inset: the relative difference of the rescaled KLF for various α_M when compared to that of $\alpha_M = 0.5$. (b) The fully diffuse boundary condition is applied with different f_{tr} . Inset: the relative difference of the rescaled KLF for various f_{tr} when compared to that of $f_{tr} = 1.85$.

and f_{tr} is essentially desired. In fact, it is ready to obtain such expressions for molecular gases by fitting the numerical data from the LBE solutions of monatomic gas as

$$\sigma_T = f_{tr}(C_1\alpha_M + C_2), \tag{33}$$

where the fitting coefficients C_1 and C_2 at various intermolecular potentials are listed in Table IV. We notice that the relative error between the fitting and numerical solutions of the model of Wu *et al.* is within 2% when $0.2 \leq \alpha_M \leq 1$ and $0.3 \leq f_{tr} \leq 2.5$. For HS molecules, the values of σ_T predicted by Eq. (3) only agree well with our simulation results when the surface is in nearly full accommodation, while the disagreement between them increases linearly with the reduction of TMAC, varying from about 2% for $\alpha_M = 1$ to approximate 13% for $\alpha_M = 0.1$. However, for Maxwellian molecules, the relative differences in σ_T are larger than 15%.

For the CL boundary condition, when α_t does not deviate too much from 1, when $|\alpha_t - 1| < 0.3$, the TSC $\sigma_T(\alpha_n, \alpha_t)$ can be expressed as

$$\sigma_T(\alpha_n, \alpha_t) = \frac{2}{5}f_{tr}\sigma_T^m(\alpha_n, \alpha_t), \tag{34}$$

where $\sigma_T^m(\alpha_n, \alpha_t)$ is the TSC for monatomic gas (see typical values in Table I). The relative error between the model of Wu *et al.* and Eq. (34) increases when α_t further deviates away from one and f_{tr} deviates away from 2.5, e.g., to 7% when $\alpha_t = 0.2$ and $f_{tr} = 0.5$.

B. The Knudsen layer function

Like the monatomic gas, the KLF of molecular gases holds similarity at different TMACs when the diffuse-specular boundary condition is applied; this is demonstrated in Fig. 9(a) where the rescaled KLFs and their relative difference are presented. It is clearly seen that the rescaled KLFs for $\alpha_M = 0.1, 0.5$, and 0.9 almost overlap with each other, and their maximum derivation from that of $\alpha_M = 0.5$

is within 3%. Additionally, the rescaled KLF is found to be well fitted by Eq. (29), with the fitting coefficients shown in Table V. The mass flow rate up to the early transition flow regime is also given by Eq. (31), where typical values of Q_d are given in the last three columns of Table V.

Interestingly, although the TSC is proportional to the translational Eucken factor f_{tr} , the rescaled KLF does not preserve the similarity with respect to f_{tr} . As presented in Fig. 9(b), the rescaled KLF profiles for $f_{tr} = 1.2, 1.85$, and 2.41 have large discrepancies. Therefore, we summarize the fitting coefficients of the rescaled KLF (29) in Table V for typical values of the viscosity index when $f_{tr} = 1.8, 2.0$, and 2.4 ; results for other parameters may be obtained through interpolation. For the CL boundary condition, the KLF does not hold the similarity at various TMACs and f_{tr} , the same as that for monatomic gases. According to Eq. (31), the break of the similarity implies that at higher Knudsen number, the mass flow rate will be different.

C. The influence of f_{tr} at large Knudsen numbers

From the above discussion, we see that the TSC of molecular gas is smaller than that of monatomic gas, especially for some polar gases where the translational Eucken factors are much smaller than 2.5, e.g., water vapor, ammonia and methanol have $f_{tr} = 1.8, 1.3$, and 0.4 , respectively.³¹ On the other hand, in the free molecular flow regime, the influence of f_{tr} on the mass flow rate will be absent due to the vanishing of collision in molecular gases. Now, we investigate the influence of f_{tr} in the intermediate transition regime. From Figs. 10(a) and 10(b), we see that the difference in mass flow rate between monatomic and molecular gases first increases with the Knudsen number, and then, it decreases when Kn increases. However, from Fig. 10(c), we see that the mass flow rate of molecular gas normalized by that of monatomic gas always decreases with the Knudsen number. These results are useful in the calibration of the capacitance diaphragm gauge when measuring low gas pressures.^{9,10}

TABLE V. Fitting coefficients of the rescaled KLF (29) and $U_d(0)$ in Eq. (30) for inverse power-law potentials with different values of viscosity index ω , when the diffuse boundary condition is used. Note that the coefficient $c_{0,0}$ is always 1 and the area under the KLF is $Q_d = \int_0^\infty U_d(x_2) dx_2$.

ω	f_{tr}	$c_{0,1}$	$-c_{0,2}$	$c_{1,0}$	$c_{1,1}$	$-c_{1,2}$	$-c_{2,0}$	$c_{2,1}$	$100c_{2,2}$	c_1	c_2	$Q_d/U_d(0)$
0.5	1.8	0.9012	0.1345	0.1832	0.4445	0.0117	0.9154	0.04059	0.0108	1.535	0.1908	1.6290
	2.0	0.8505	0.1368	0.1519	0.4303	0.0119	0.8707	0.04173	0.0102	1.375	0.2485	1.7018
	2.4	0.7697	0.1367	0.1071	0.4090	0.0114	0.8012	0.04102	0.0087	1.354	0.3260	1.8408
0.75	1.8	1.0140	0.2394	0.6123	0.6975	0.0216	1.3300	0.07534	0.0195	1.346	0.2579	1.7783
	2.0	0.9602	0.2340	0.5597	0.6703	0.0208	1.2640	0.07318	0.0178	1.324	0.3038	1.8042
	2.4	0.8741	0.2226	0.4807	0.6280	0.0190	1.1620	0.06799	0.0150	1.340	0.3867	1.9412
1.0	1.8	1.1600	0.3745	1.1480	1.0160	0.0344	1.8510	0.12070	0.0294	1.285	0.3162	1.8511
	2.0	1.1020	0.3619	1.0730	0.9738	0.0329	1.7640	0.11600	0.0274	1.301	0.3603	1.9232
	2.4	1.0050	0.3333	0.9438	0.9018	0.0287	1.6120	0.10320	0.0220	1.366	0.4402	2.0617
1.25	1.8	1.3340	0.5374	1.7890	1.4000	0.0489	2.4760	0.17350	0.0386	1.280	0.3678	1.9993
	2.0	1.2670	0.5095	1.6710	1.3330	0.0452	2.3460	0.16180	0.0344	1.322	0.4106	2.0733
	2.4	1.1580	0.4653	1.4900	1.2290	0.0396	2.1430	0.14370	0.0284	1.422	0.4882	2.2156

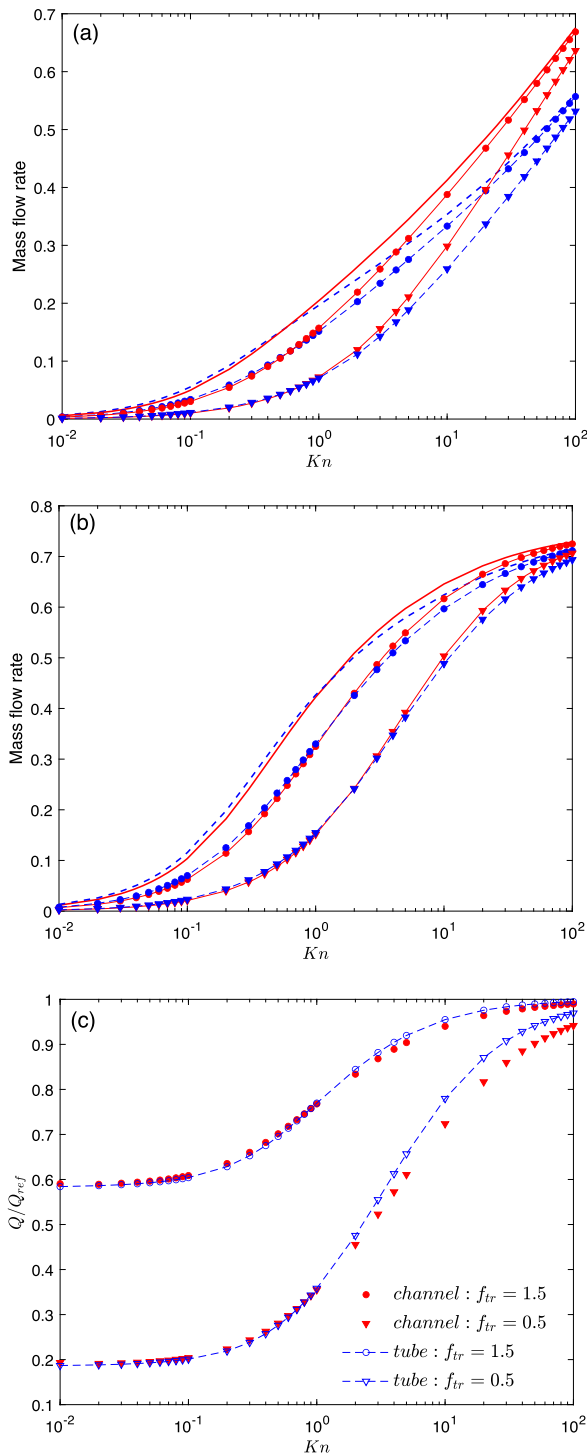


FIG. 10. The mass flow rate Q as a function of Knudsen number through a planar channel (a) and tube (b). Solid lines: HS gas. Dashed lines: Maxwellian gas. The translational Eucken factors corresponding to lines, circles, and triangles are $f_{tr} = 2.5, 1.5,$ and 0.5 . (c) The mass flow rate as compared to that of monatomic gas Q_{ref} when the HS gas model is used. The results of Maxwell gases almost overlap with those of HS gases.

V. COMPARISON WITH EXPERIMENTS

The experimental data on thermal transpiration of air and carbon dioxide in a circular tube are now examined by the LBE calculations. From the discussions in previous sections, we know that these data depend on the values of f_{tr} , ω , and TMAC. The same problem has been investigated by Loyalka *et al.*⁴² based on the model of Hanson and Morse⁴⁰ that is derived from the Wang-Chang and Uhlenbeck equation⁴¹ for Maxwellian molecules, but with the diffuse boundary condition only. The methodology we will adopt has two major advantages. First, in the model of Wu *et al.*⁵⁰ for molecular gases, the viscosity index can be properly chosen to reflect the intermolecular potential for each gas, which is not accessible in previous molecular gas models. Second, f_{tr} is extracted from the experiments of Rayleigh–Brillouin scattering, where the gas–surface interaction is absent so that it is obtained accurately.⁵² Therefore, in the comparison between our LBE and experiential results, the gas–surface boundary condition in thermal transpiration can be extracted with good accuracy.

A. The TPD exponent

In the experiment of thermal transpiration, usually, the TPD exponent γ is measured. When the temperature ratio of two gas reservoirs connected by a long circular tube is small, the TPD exponent can be calculated as

$$\gamma = -\frac{Q_T}{Q_P}, \tag{35}$$

where Q_T and Q_P are the mass flow rates along the tube in thermal transpiration and Poiseuille flows, respectively.

In the slip regime, with the aid of the first-order slip boundary condition, the dimensionless mass flow rate of the Poiseuille flow Q_P in a circular tube is⁷⁰

$$Q_P = \frac{\delta_{rp}}{8} + \frac{\sigma_P}{2}, \tag{36}$$

where the VSC is set to $\sigma_P = 1, 1.2,$ and 1.46 for the cases of $\alpha_M = 1, 0.9,$ and $0.8,$ respectively, as the intermolecular potential has negligible effect on these values.²⁴ Note that Eq. (36) is accurate when $\delta > 10$. With Eq. (31), the analytical solution of the TPD exponent in the slip regime can be written as

$$\gamma = \frac{4\sigma_T\delta_{rp} - 2\pi Q_d}{\delta_{rp}^2(\delta_{rp} + 4\sigma_P)}. \tag{37}$$

In our LBE simulations, the viscosity index ω for each gas is set according to the gaseous property.¹⁶ With the values of Q_d , σ_T , and σ_P at a specific α_M obtained from previous sections, the analytical solution (37) for the TPD exponent can be determined, which will be used to extract the TMAC by comparing with the experimental data when $\delta_{rp} > 3.5$. Then, we solve the model of Wu *et al.* toward smaller values of $\delta_{rp} < 3.5$ to see whether our results still agree with experimental data or not.

B. Air

We first compare the calculated TPD exponent of thermal transpiration for air with the experimental data by Arney and Bailey⁷¹ in Fig. 11. Since air is mainly the mixture of nitrogen and oxygen,

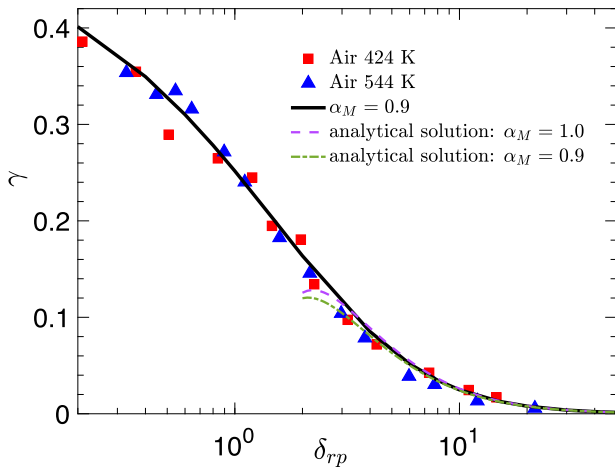


FIG. 11. TPD exponent vs the rarefaction parameter δ_{rp} for air flows along a circular tube. Symbols: experimental data extracted from Ref. 71. Black lines: numerical solutions of the model of Wu *et al.*⁵⁰ The analytical solution is given by Eq. (37).

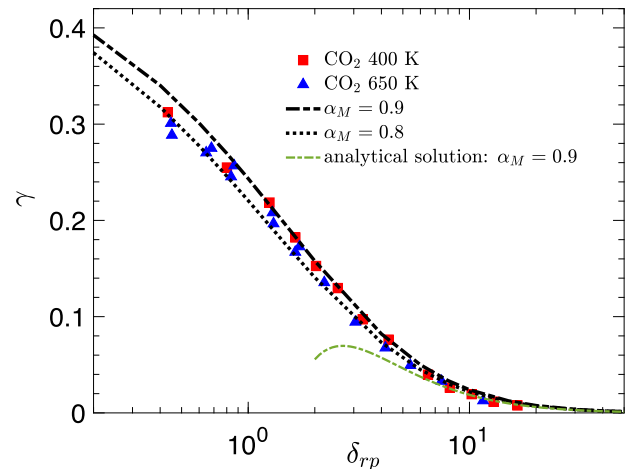


FIG. 12. The same as Fig. 11 except that now, CO_2 is used.⁷²

an effective viscosity index of $\omega = 0.75$ is chosen to reproduce the proper intermolecular potential of the air molecules.^{16,24} The number of rotational degrees is $d = 2$. The translational Eucken factor is $f_{tr} = 2.4$ as extracted from the Rayleigh–Brillouin experiments of nitrogen.⁵² We first use the analytical expression (37) to obtain the TMAC by comparing with the experimental data at $\delta > 10$. From the results in previous sections, the TSC can be extracted from the linear function

$$\sigma_T = 0.294\alpha_M + 0.752, \quad (38)$$

and the mass flow rate correction Q_d for air can be calculated from

$$Q_d = 4.182[1 - \exp(-0.228\alpha_M)]. \quad (39)$$

We find that when α_M varies from 0.8 to 1, the results in Eq. (37) can cover almost all the experimental data at temperature $T = 424$ K and 544 K. Then, we solve the Wu *et al.* model over a wide range of rarefaction parameter and find that the TMAC in the air experiments is more likely 0.9, rather than $\alpha_M = 1$ used in Ref. 42.

C. Carbon dioxide

The comparisons of the TPD exponent for CO_2 between the measurements and solutions of the model of Wu *et al.* are shown in Fig. 12, where the effective viscosity index is set to 0.93, while the translational Eucken factor is $f_{tr} = 2.24$ as extracted from the Rayleigh–Brillouin experiments of carbon dioxide.⁵² The rotational degrees is still equal to 2, since the three atoms in a CO_2 molecule line up. We estimate the values of TSC and the mass flow correction Q_d as

$$\begin{aligned} \sigma_T &= 0.271\alpha_M + 0.576, \\ Q_d &= 4.726[1 - \exp(-0.207\alpha_M)]. \end{aligned} \quad (40)$$

We can also see that, when $\delta_{rp} > 1$, the experimental data at $T = 400$ K can be well reproduced by the model of Wu *et al.* when $\alpha_M = 0.9$, while the data at a higher temperature of $T = 650$ are

more close to solutions of the model of Wu *et al.* when $\alpha_M = 0.8$. Note that the value of γ at $\delta_{rp} \approx 0.45$ is even below the profile of $\alpha_M = 0.8$, which may be attributed to the inaccurate experimental measurement at low gas pressures. Nevertheless, all experimental data almost fall between the profiles of $\alpha_M = 0.8$ and 0.9, which suggest that the TMAC in the CO_2 experiment is more likely $\alpha_M = 0.85 \pm 0.05$.

VI. CONCLUSIONS

The thermal transpiration of molecular gas between two parallel plates and along cylinder tubes has been investigated based on the model of Wu *et al.*,⁵⁰ where the elastic and inelastic collisions are modeled by the Boltzmann and Rykov⁴⁶ collision operators, respectively. In the limit of no inelastic collision, such a model is reduced to the Boltzmann equation so that the role of intermolecular potential can be investigated. A synthetic iteration scheme is proposed to find the steady-state solutions within dozens of iterations, which is about two to three orders of magnitude faster than the conventional iterative method in the transition and near-continuum flow regimes. With this efficient and accurate method, the influence of intermolecular potential and internal structure of molecular gases on the mass flow rate and Knudsen layer function of thermal transpiration has been studied systematically.

The role of intermolecular potential is reflected in the viscosity index, which strongly affects the TSC and KLF. In numerical simulations of monatomic gas, we found that the TSC and KLF increase with the viscosity index, except in the cases where the TMAC approaches zero (rare in real materials). When the viscosity index is fixed for the diffuse–specular boundary condition, the TSC increases linearly with TMAC. However, the TSC is a nonlinear function of the TMAC α_i in the CL boundary condition. We have observed that the KLF holds similarities when the diffuse–specular boundary condition is applied, i.e., $U_d/U_d(x_2 = 0)$ almost overlaps with each other when TMAC changes; this similarity is slightly broken when the CL boundary condition is used. For molecular gas, we

have found that the ratio of TSC between molecular and monatomic gases is approximately the ratio of their translational Eucken factors. Therefore, for some polar gases where the translational Eucken factor is much smaller than 2.5 of monatomic gas, the mass flow rate of thermal transpiration can be much reduced.

An analytical expression of mass flow rate in thermal transpiration is established up to the early transition regime, and values of TSC and KLF (hence Q_d) are tabulated for typical viscosity index, accommodation coefficients in gas-kinetic boundary conditions, and translational Eucken factor. This expression may be helpful for engineering applications. With the utilization of a more realistic intermolecular potential, we have found that the TMACs extracted from the thermal transpiration experiments of air and carbon dioxide along circular tubes are 0.9 and 0.85, respectively, rather than one used in the literature. Also, the data presented in this paper are useful, for example, in the pressure calibration of the capacitance diaphragm gauge when measuring low gas pressures.

ACKNOWLEDGMENTS

This work was supported by the Engineering and Physical Sciences Research Council in the UK under Grant No. EP/R041938/1. P. Wang acknowledges the financial support by the Fundamental Research Funds for the Central Universities, HUST (Grant No. 2020kfyXJJS070).

DATA AVAILABILITY

The data that support the findings of this study are available from the corresponding author upon reasonable request.

REFERENCES

- O. Reynolds, "XVIII. On certain dimensional properties of matter in the gaseous state. Part I. Experimental researches on thermal transpiration of gases through porous plates and on the laws of transpiration and impulsion, including an experimental proof that gas is not a continuous plenum. Part II. On an extension of the dynamical theory of gas, which includes the stresses, tangential and normal, caused by a varying condition of gas, and affords an explanation of the phenomena of transpiration and impulsion," *Philos. Trans. R. Soc. London* **170**, 727–845 (1879).
- J. C. Maxwell, "VII. On stresses in rarified gases arising from inequalities of temperature," *Philos. Trans. R. Soc. London* **170**, 231–256 (1879).
- W. Crookes, "XV. On attraction and repulsion resulting from radiation," *Philos. Trans. R. Soc. London* **164**, 501–527 (1874).
- J. Xie, C. K. Lee, and H. H. Feng, "Design, fabrication, and characterization of CMOS MEMS-based thermoelectric power generators," *J. Microelectromech. Syst.* **19**, 317–324 (2010).
- A. Ventura, N. Gimelshein, S. Gimelshein, and A. Ketsdever, "Effect of vane thickness on radiometric force," *J. Fluid Mech.* **735**, 684–704 (2013).
- A. Strongrich, A. Pikus, I. B. Sebastião, and A. Alexeenko, "Microscale in-plane Knudsen radiometric actuator: Design, characterization, and performance modeling," *J. Micromech. Microeng.* **26**, 528–538 (2017).
- S. E. Vargo, E. P. Muntz, G. R. Shifflett, and W. C. Tang, "Knudsen compressor as a micro- and macroscale vacuum pump without moving parts or fluids," *J. Vac. Sci. Technol., A* **17**, 2308–2313 (1999).
- N. K. Gupta and Y. B. Gianchandani, "Thermal transpiration in zeolites: A mechanism for motionless gas pumps," *Appl. Phys. Lett.* **93**, 193511 (2008).
- J. Sentina, "New approach to corrections for thermal transpiration effects in capacitance diaphragm gauges," *Metrologia* **36**, 623–626 (1999).
- B. Daudé, H. Elandaloussi, and C. Janssen, "On the gas dependence of thermal transpiration and a critical appraisal of correction methods for capacitive diaphragm gauges," *Vacuum* **104**, 77–87 (2014).
- S. Takata, H. Sugimoto, and S. Kosuge, "Gas separation by means of the Knudsen compressor," *Eur. J. Mech.: B/Fluids* **26**, 155–181 (2007).
- A. Würger, "Leidenfrost gas ratchets driven by thermal creep," *Phys. Rev. Lett.* **107**, 164502 (2011).
- F. G. Tcheremissine, "Direct numerical solution of the Boltzmann equation," *AIP Conf. Proc.* **762**, 677–685 (2005).
- L. Wu, J. M. Reese, and Y. H. Zhang, "Solving the Boltzmann equation by the fast spectral method: Application to microflows," *J. Fluid Mech.* **746**, 53–84 (2014).
- W. Su, L. H. Zhu, P. Wang, Y. H. Zhang, and L. Wu, "Can we find steady-state solutions to multiscale rarefied gas flows within dozens of iterations?," *J. Comput. Phys.* **407**, 109245 (2020).
- G. A. Bird, *Molecular Gas Dynamics and the Direct Simulation of Gas Flows* (Oxford Science Publications, Oxford University Press, Inc., New York, 1994).
- G. A. Radtke, N. G. Hadjiconstantinou, and W. Wagner, "Low-noise Monte Carlo simulation of the variable hard sphere gas," *Phys. Fluids* **23**, 030606 (2011).
- Y. Sone, *Kinetic Theory and Fluid Dynamics* (Birkhäuser Boston, 2002).
- F. Sharipov and V. Seleznev, "Data on internal rarefied gas flows," *J. Phys. Chem. Ref. Data* **27**, 657–706 (1998).
- D. A. Lockerby, J. M. Reese, D. R. Emerson, and R. W. Barber, "Velocity boundary condition at solid walls in rarefied gas calculations," *Phys. Rev. E* **70**, 017303 (2004).
- V. Leontidis, J. Chen, L. Baldas, and S. Colin, "Numerical design of a Knudsen pump with curved channels operating in the slip flow regime," *Heat Mass Transfer* **50**, 1065–1080 (2014).
- T. Ohwada, Y. Sone, and K. Aoki, "Numerical analysis of the shear and thermal creep flows of a rarefied gas over a plane wall on the basis of the linearized Boltzmann equation for hard-sphere molecules," *Phys. Fluids A* **1**, 1588–1599 (1989).
- C. E. Siewert, "Viscous-slip, thermal-slip, and temperature-jump coefficients as defined by the linearized Boltzmann equation and the Cercignani-Lampis boundary condition," *Phys. Fluids* **15**, 1696–1701 (2003).
- W. Su, P. Wang, H. H. Liu, and L. Wu, "Accurate and efficient computation of the Boltzmann equation for Couette flow: Influence of intermolecular potentials on Knudsen layer function and viscous slip coefficient," *J. Comput. Phys.* **378**, 573–590 (2019).
- B. K. Annis, "Thermal creep in gases," *J. Chem. Phys.* **57**, 2898–2905 (1972).
- B. T. Porodnov, A. N. Kulev, and F. T. Tuchvetov, "Thermal transpiration in a circular capillary with a small temperature difference," *J. Fluid Mech.* **88**, 609–622 (1978).
- M. Rojas-Cárdenas, I. Graur, P. Perrier, and J. G. Méolans, "A new method to measure the thermal slip coefficient," *Int. J. Heat Mass Transfer* **88**, 766–774 (2015).
- H. Yamaguchi, P. Perrier, M. T. Ho, J. G. Méolans, T. Niimi, and I. A. Graur, "Mass flow rate measurement of thermal creep flow from transitional to slip flow regime," *J. Fluid Mech.* **795**, 690–707 (2016).
- S. K. Loyalka, "Slip and jump coefficients for rarefied gas flows: Variational results for Lennard-Jones and $n(r)$ -6 potentials," *Physica A* **163**, 813–821 (1990).
- F. Sharipov, "Data on the velocity slip and temperature jump on a gas-solid interface," *J. Phys. Chem. Ref. Data* **40**, 023101 (2011).
- E. A. Mason and L. Monchick, "Heat conductivity of polyatomic and polar gases," *J. Chem. Phys.* **36**, 1622 (1962).
- F. Sharipov and G. Bertoldo, "Poiseuille flow and thermal creep based on the Boltzmann equation with the Lennard-Jones potential over a wide range of the Knudsen number," *Phys. Fluids* **21**, 067101 (2009).
- L. Wu, H. H. Liu, Y. H. Zhang, and J. M. Reese, "Influence of intermolecular potentials on rarefied gas flows: Fast spectral solutions of the Boltzmann equation," *Phys. Fluids* **27**, 082002 (2015).
- S. K. Loyalka, N. Petrellis, and T. S. Storvick, "Some numerical results for the BGK model: Thermal creep and viscous slip problems with arbitrary accommodation at the surface," *Phys. Fluids* **18**, 1094–1099 (1975).

- ³⁵S. K. Loyalka and T. S. Storvick, "Kinetic theory of thermal transpiration and mechanocaloric effect. III. Flow of a polyatomic gas between parallel plates," *J. Chem. Phys.* **71**, 339–350 (1979).
- ³⁶C. E. Siewert and F. Sharipov, "Model equations in rarefied gas dynamics: Viscous-slip and thermal-slip coefficients," *Phys. Fluids* **14**, 4123–4129 (2002).
- ³⁷E. A. Mason, "Molecular relaxation times from thermal transpiration measurements," *J. Chem. Phys.* **39**, 522–526 (1963).
- ³⁸A. D. Gupta and T. S. Storvick, "Analysis of the heat conductivity data for polar and nonpolar gases using thermal transpiration measurements," *J. Chem. Phys.* **52**, 742–749 (1970).
- ³⁹P. L. Bhatnagar, E. P. Gross, and M. Krook, "A model for collision processes in gases. I. Small amplitude processes in charged and neutral one-component systems," *Phys. Rev.* **94**, 511–525 (1954).
- ⁴⁰F. B. Hanson and T. F. Morse, "Kinetic models for a gas with internal structure," *Phys. Fluids* **10**, 345–353 (1967).
- ⁴¹C. S. Wang-Chang and G. E. Uhlenbeck, "Transport phenomena in polyatomic gases," Report No. CM-681, University of Michigan Engineering Research, 1951.
- ⁴²S. K. Loyalka, T. S. Storvick, and S. S. Lo, "Thermal transpiration and mechanocaloric effect. IV. Flow of a polyatomic gas in a cylindrical tube," *J. Chem. Phys.* **76**, 4157–4170 (1982).
- ⁴³S. S. Lo and S. K. Loyalka, "Flow of a rarefied polyatomic gas between parallel plates," *J. Vac. Sci. Technol., A* **7**, 2766–2773 (1989).
- ⁴⁴L. H. Holway, "New statistical models for kinetic theory: Methods of construction," *Phys. Fluids* **9**, 1658–1673 (1966).
- ⁴⁵P. Andries, P. Le Tallec, J.-P. Perlat, and B. Perthame, "The Gaussian-BGK model of Boltzmann equation with small Prandtl number," *Eur. J. Mech.: B/Fluids* **19**, 813–830 (2000).
- ⁴⁶V. Rykov, "A model kinetic equation for a gas with rotational degrees of freedom," *Fluid Dyn.* **10**, 959–966 (1975).
- ⁴⁷A. S. Fernandes and W. Marques, "Kinetic model analysis of time-dependent problems in polyatomic gases," *Physica A* **373**, 97–118 (2007).
- ⁴⁸C. Tantos, D. Valougeorgis, M. Pannuzzo, A. Frezzotti, and G. L. Morini, "Conductive heat transfer in a rarefied polyatomic gas confined between coaxial cylinders," *Int. J. Heat Mass Transfer* **79**, 378–389 (2014).
- ⁴⁹C. Tantos, D. Valougeorgis, and A. Frezzotti, "Conductive heat transfer in rarefied polyatomic gases confined between parallel plates via various kinetic models and the DSMC method," *Int. J. Heat Mass Transfer* **88**, 636–651 (2015).
- ⁵⁰L. Wu, C. White, T. J. Scanlon, J. M. Reese, and Y. H. Zhang, "A kinetic model of the Boltzmann equation for non-vibrating polyatomic gases," *J. Fluid Mech.* **763**, 24–50 (2015).
- ⁵¹M. A. Gallis, D. J. Rader, and J. R. Torczynski, "A generalized approximation for the thermophoretic force on a free-molecular particle," *Aerosol Sci. Technol.* **38**, 692–706 (2004).
- ⁵²L. Wu, Q. Li, H. H. Liu, and W. Ubachs, "Extraction of the translational Eucken factor from light scattering by molecular gas," *J. Fluid Mech.* (published online 2020).
- ⁵³C. Borgnakke and P. S. Larsen, "Statistical collision model for Monte Carlo simulation of polyatomic gas mixture," *J. Comput. Phys.* **18**, 405–420 (1975).
- ⁵⁴S. Chapman and T. G. Cowling, *The Mathematical Theory of Non-Uniform Gases* (Cambridge University Press, 1970).
- ⁵⁵C. Cercignani, *The Boltzmann Equation and Its Applications* (Springer, 1988).
- ⁵⁶L. Wu, C. White, T. J. Scanlon, J. M. Reese, and Y. H. Zhang, "Deterministic numerical solutions of the Boltzmann equation using the fast spectral method," *J. Comput. Phys.* **250**, 27–52 (2013).
- ⁵⁷When the intermolecular potential varies as $r^{-\eta}$ with r being the intermolecular distance, the shear viscosity μ of the gas is proportional to T^ω , with $\omega = (\eta + 3)/2(\eta - 1)$.⁵⁴
- ⁵⁸C. Cercignani and M. Lampis, "Kinetic models for gas-surface interactions," *Transp. Theory Stat. Phys.* **1**(2), 101–114 (1971).
- ⁵⁹R. G. Lord, "Some extensions to the Cercignani–Lampis gas–surface scattering kernel," *Phys. Fluids A* **3**, 706–710 (1991).
- ⁶⁰D. Valougeorgis and S. Naris, "Acceleration schemes of the discrete velocity method: Gaseous flows in rectangular microchannels," *SIAM J. Sci. Comput.* **25**, 534–552 (2003).
- ⁶¹L. Wu, J. Zhang, H. H. Liu, Y. H. Zhang, and J. M. Reese, "A fast iterative scheme for the linearized Boltzmann equation," *J. Comput. Phys.* **338**, 431–451 (2017).
- ⁶²W. Su, M. T. Ho, Y. H. Zhang, and L. Wu, "GSIS: An efficient and accurate numerical method to obtain the apparent gas permeability of porous media," *Comput. Fluids* **206**, 104576 (2020).
- ⁶³M. Wakabayashi, T. Ohwada, and F. Golse, "Numerical analysis of the shear and thermal creep flows of a rarefied gas over the plane wall of a Maxwell-type boundary on the basis of the linearized Boltzmann equation for hard-sphere molecules," *Eur. J. Mech.: B/Fluids* **15**, 175–201 (1996).
- ⁶⁴C. E. Siewert, "The linearized Boltzmann equation: Concise and accurate solutions to basic flow problems," *Z. Angew. Math. Phys.* **54**, 273–303 (2003).
- ⁶⁵F. Sharipov, "Application of the Cercignani–Lampis scattering kernel to calculations of rarefied gas flows. II. Slip and jump coefficients," *Eur. J. Mech.: B/Fluids* **22**, 133–143 (2003).
- ⁶⁶E. M. Shakhov, "Generalization of the Krook kinetic relaxation equation," *Fluid Dyn.* **3**, 95–96 (1968).
- ⁶⁷S. Takata and H. Funagane, "Singular behaviour of a rarefied gas on a planar boundary," *J. Fluid Mech.* **717**, 30–47 (2013).
- ⁶⁸S. Takata and S. Taguchi, "Gradient divergence of fluid-dynamic quantities in rarefied gases on smooth boundaries," *J. Stat. Phys.* **168**, 1319–1352 (2017).
- ⁶⁹S. Jiang and L.-S. Luo, "Analysis and accurate numerical solutions of the integral equation derived from the linearized BGKW equation for the steady Couette flow," *J. Comput. Phys.* **316**, 416–434 (2016).
- ⁷⁰F. Sharipov, *Rarefied Gas Dynamics: Fundamentals for Research and Practice* (John Wiley & Sons, 2015).
- ⁷¹G. D. Arney and A. B. Bailey, "An investigation of the equilibrium pressure along unequally heated tubes," Technical Report AEDC-TDR-62-188, Arnold Engineering Development Center, Arnold Air Force Station, TN, 1962.
- ⁷²T. S. Storvick, H. S. Park, and S. K. Loyalka, "Thermal transpiration: A comparison of experiment and theory," *J. Vac. Sci. Technol.* **15**, 1844–1852 (1978).